

Useful island block geometries of a passive intensity modulator used for intensity-modulated bolus electron conformal therapy

Erin L. Chambers¹ | Robert L. Carver^{1,2} | Kenneth R. Hogstrom^{1,2}

¹Department of Physics and Astronomy,
Louisiana State University, Baton Rouge,
LA, USA

²Mary Bird Perkins Cancer Center, Baton
Rouge, LA, USA

Authors to whom correspondence should be
addressed: Robert L. Carver

E-mail: rcarver@marybird.com

Telephone: 225-215-1180; Fax: 225-215-
1376

Abstract

Purpose: This project determined the range of island block geometric configurations useful for the clinical utilization of intensity-modulated bolus electron conformal therapy (IM-BECT).

Methods: Multiple half-beam island block geometries were studied for seven electron energies 7–20 MeV at 100 and 103 cm source-to-surface distance (SSD). We studied relative fluence distributions at 0.5 cm and 2.0 cm depths in water, resulting in 28 unique beam conditions. For each beam condition, we studied intensity reduction factor (IRF) values of 0.70, 0.75, 0.80, 0.85, 0.90, and 0.95, and hexagonal packing separations for the island blocks of 0.50, 0.75, 1.00, 1.25, and 1.50 cm, that is, 30 unique IM configurations and 840 unique beam-IM combinations. A combination was deemed acceptable if the average intensity downstream of the intensity modulator agreed within 2% of that intended and the variation in fluence was less than $\pm 2\%$.

Results: For 100 cm SSD, and for 0.5 cm depth, results showed that beam energies above 13 MeV did not exhibit sufficient scatter to produce clinically acceptable fluence (intensity) distributions for all IRF values (0.70–0.95). In particular, 20 MeV fluence distributions were unacceptable for any values, and acceptable 16 MeV fluence distributions were limited to a minimum IRF of 0.85. For the 2.0 cm depth, beam energies up to and including 20 MeV had acceptable fluence distributions. For 103 cm SSD and for 0.5 cm and 2.0 cm depths, results showed that all beam energies (7–20 MeV) had clinically acceptable fluence distributions for all IRF values (0.70–0.95). In general, the more clinically likely 103 cm SSD had acceptable fluence distributions with larger separations (r), which allow larger block diameters.

Conclusion: The geometric operating range of island block separations and IRF values (block diameters) producing clinically appropriate IM electron beams has been determined.

KEY WORDS

electron therapy, intensity modulation, bolus, conformal therapy

1 | INTRODUCTION

Electron beam therapy has been a standard modality in radiation treatment for over 60 years. Electron beams with energies between 6 and 20 MeV ($R_{90} = 1.8\text{--}6.0$ cm) are characterized by high surface dose, relatively uniform dose plateau, sharp distal dose fall off, and low exit x-ray dose. These characteristics have allowed superficial cancers within 6 cm of surface to be treated while minimizing dose to underlying critical structures.¹ Historically, electrons have been the modality of choice for (1) the treatment of skin, lip, and head and neck tumors, (2) boost doses to superficial lymph nodes, and (3) post-mastectomy chest wall irradiation.^{2–5} Electron therapy planning often utilizes a single beam of energy just sufficient for R_{90} of the electron beam to exceed maximum planning target volume (PTV) depth. However, delivery is often complicated by internal

heterogeneities, irregular patient surface, and variable depth of the distal PTV surface resulting in needless overdosing of distal structures, in which case some form of electron conformal therapy (ECT) is desirable.⁶

The goals of electron conformal therapy are to conform the distal 90% dose surface to the distal surface of the PTV, provide a homogeneous or prescribed heterogeneous dose to the PTV, and maximize dose sparing of critical structures deep to the PTV.⁶ One of three methods described by Hogstrom et al.⁶ is Bolus ECT, which uses a single energy electron beam to deliver a dose distribution that conforms the 90% dose surface to the distal surface of the PTV. This is accomplished by using variable-thickness bolus, a nearly water-equivalent material which is placed on the patient surface. Algorithms for bolus design were first created by Low et al.⁷ and later by Su et al.⁸; these algorithms projected ray lines from the electron virtual source to the distal margin of the PTV and applied a succession of bolus operators to generate a bolus structure. Fig. 1

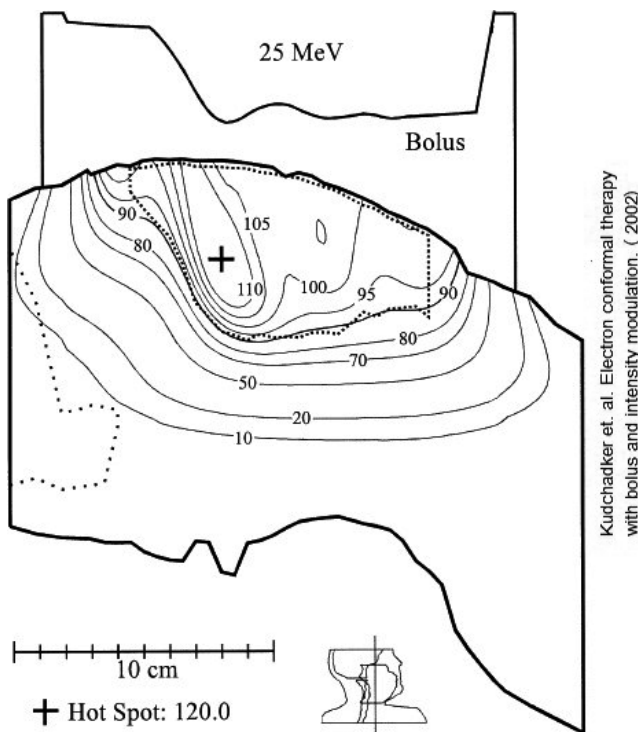


FIG. 1. Isodosedistribution (100% = given dose) for a 25 MeV bolus ECT treatment plan of a right buccal mucosa patient; 90% dose surface conforms to the distal surface of the planning target volume (dotted line). From Kudchadker et al (2003).

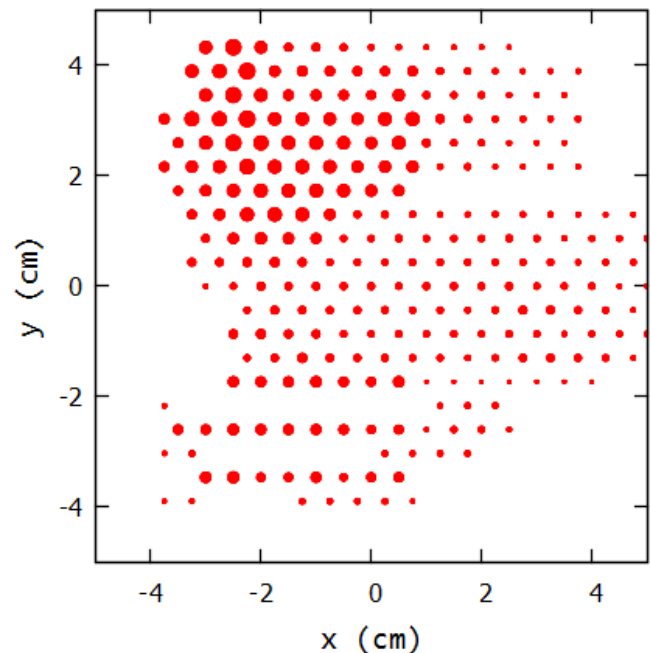


FIG. 2. Beam's eye view of intensity modulator design for the buccal mucosa patient shown in Fig.1. Red circles show variable circular cross sections of island blocks.

TABLE 1 Island block diameters (d) in cm for select combinations of intensity reduction factors (IRF) and hexagonal island block separations (r) calculated using Equation 1.

IRF	$r = 0.5$ cm	$r = 0.75$ cm	$r = 1.0$ cm	$r = 1.25$ cm	$r = 1.5$ cm
0.95	0.117	0.176	0.235	0.294	0.352
0.90	0.166	0.249	0.332	0.415	0.498
0.85	0.203	0.305	0.407	0.508	0.610
0.80	0.235	0.352	0.470	0.587	0.704
0.75	0.263	0.394	0.525	0.656	0.788
0.70	0.288	0.431	0.575	0.719	0.863

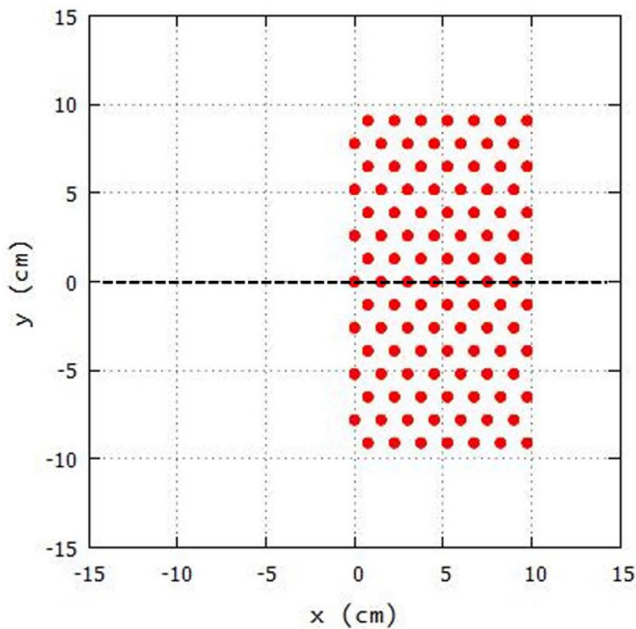


FIG. 3. Sample island block matrix used to determine acceptable (r, d) combinations. For this example, blocks with (r, d) = (1.50 cm, 0.498 cm), having an IRF = 0.90, are hexagonally packed in the + x half plane of the $20 \times 20 \text{ cm}^2$ field at the positions indicated by the red circles. Red circles show circular cross sections of island blocks. Dashed line at $y=0$ indicates the xz plane in which off-axis profiles of relative intensity versus x were calculated at depths of $z = 0.5$ and 2.0 cm in water.

illustrates how bolus ECT conforms the 90% dose surface to the distal PTV surface of a right buccal mucosa patient. Boluses have been readily available to clinics since the introduction in 2009 of bolus design software (BolusECT[®]) in the p.d software system and bolus fabrication using milling technology, available from decimal, LLC (Sanford, FL, <http://dotdecimal.com/products/electrons/bolussect/>). BolusECT[®] utilizes design operators based on Low et al.⁷ and a pencil beam redefinition algorithm for dose calculations,^{9–12} which has been verified for patient-like volumes.

Bolus ECT has been used for multiple sites, which include posterior chest wall^{8,13,14}; post-mastectomy chest wall^{14–17}; ear, parotid, and buccal mucosa,^{14,18} nose,¹⁹ and extremities (hand and foot).⁸ The irregular upstream bolus surface can often cause undesirable dose heterogeneities in the PTV. However, it was shown by Kudchadker et al.¹⁴ that the introduction of modest intensity modulation (70%–100%) across the beam can significantly reduce PTV heterogeneity for some patients.

Initially, delivery of intensity modulation was envisioned using eMLCs, such as those reported by Hogstrom et al.²⁰ and Gauer et al.²¹; however, access to said devices by the typical clinic has not been forthcoming. As an alternative, Hogstrom et al.²² reported a passive method for electron intensity modulation, which consists of a matrix of variable small-diameter, high-density island blocks, as shown in Fig. 2. The matrix consists of small diameter, tungsten cylinders (eg 0.2 to 0.6 cm diameter \times 0.6 cm thick) of varying diameter placed on a hexagonal grid with

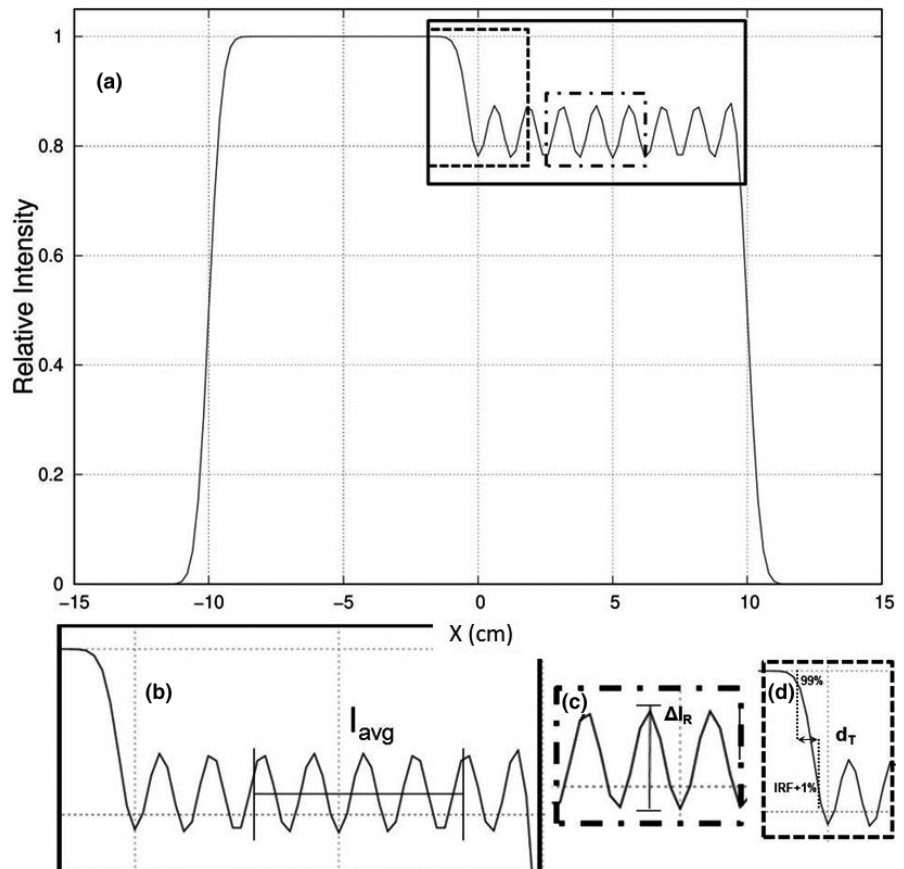


FIG. 4. Illustrations of the assessment metrics. (a) Relative intensity vs. x -position profile ($y = 0$ cm) for $E = 13$ MeV, $FS = 20 \times 20 \text{ cm}^2$, source-to-surface distance (SSD) = 100 cm, depth $z = 2.0$ cm is plotted for a matrix of island blocks at locations shown in Fig. 3, with island block parameters of $r = 1.25$ cm and $d = 0.415$ cm (IRF = 0.85). (b) I_{avg} is the average intensity in the specified region. (c) ΔI_R is the maximum spread in the specified region. (d) Distance of transition (d_T) is the distance from the 99% to the (IRF-1%) relative intensity.

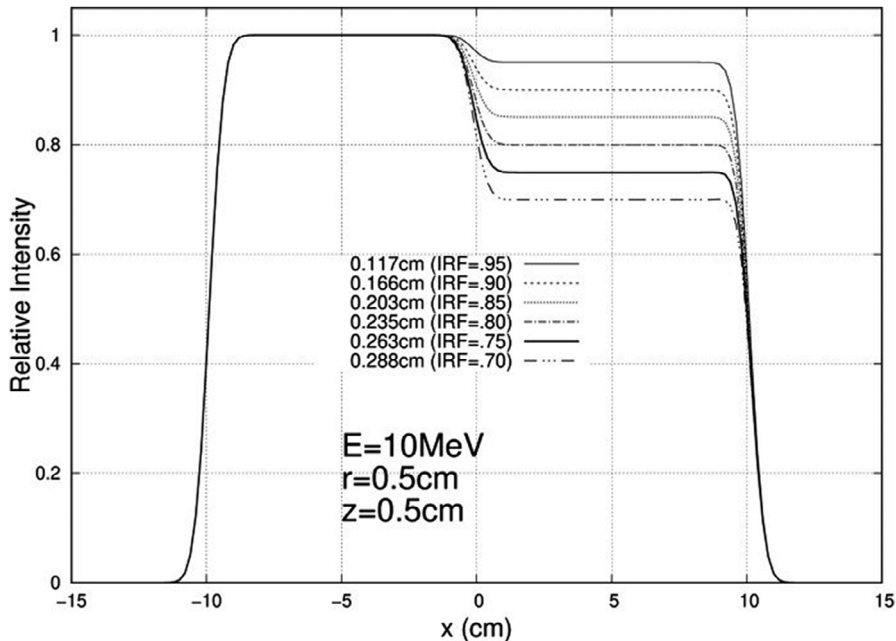
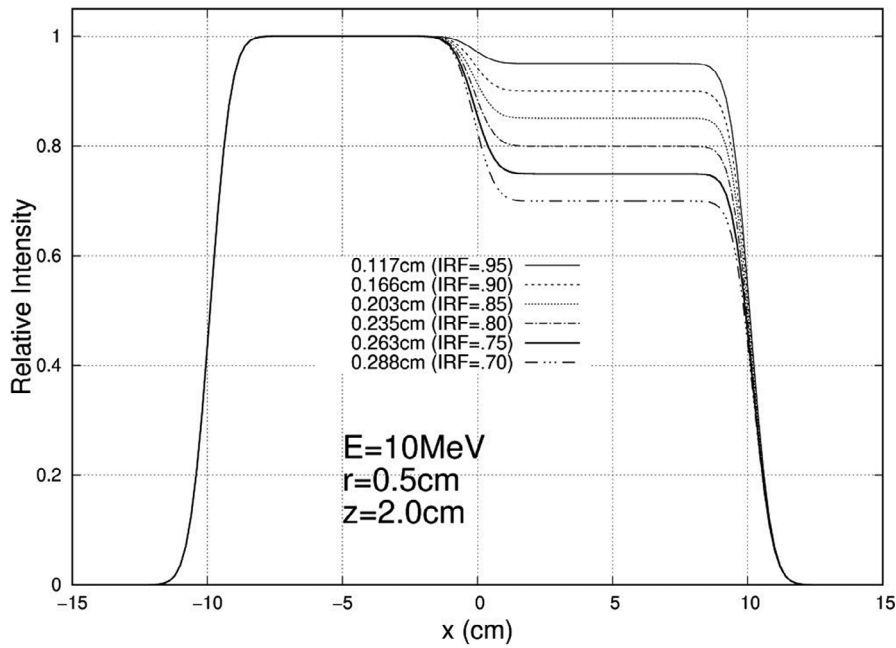


FIG. 5. Profiles at $y = 0$ cm for 10 MeV, 20×20 cm² half-modulated field ($r = 0.5$ cm), 103 cm source-to-surface distance (SSD): depth $z = 0.5$ cm (top) and $z = 2.0$ cm (bottom). The computed island block diameters (d) for 0.70, 0.75, 0.80, 0.85, 0.90, and 0.95 IRF values are listed in each plot's inserted key.

approximately 0.6 cm spacing. The cylinders, referred to as island blocks and whose axes follow diverging fan lines, are embedded in a low density machineable foam (≈ 0.1 g*cm⁻³) that fits inside the aperture of the electron beam cutout located in the bottom of the electron applicator. The matrix can closely produce the desired intensity modulation while the beam energy remains almost unchanged (≈ 0.2 MeV decrease due to the foam substrate on which island blocks are mounted²³). The local beam intensity is determined by the fraction of the beam locally removed by the island blocks. Because of the multiple Coulomb scattering (MCS) of the electron beam, fluence is filled in behind the blocks 5–10 cm downstream. Using small diameter islands blocks,

intensity modulators can be designed for suitable intensity-modulated bolus electron conformal therapy (IM-BECT).

The purpose of this study was to investigate how best to deliver passive intensity modulation for IM-BECT, where intensity modulation in the range of 70%–100% should be sufficient. Intensity modulation using island blocks can be achieved by either modifying the diameter and/or spacing of the island blocks. Our study only investigates island blocks placed on a hexagonal grid and then varying their diameters to achieve the appropriate IM, as illustrated in Fig. 2.

The fraction of area locally blocked, which controls the intensity reduction factor (IRF) locally, is governed by the ratio of block diameter (d) to hexagonal grid spacing (r),²²

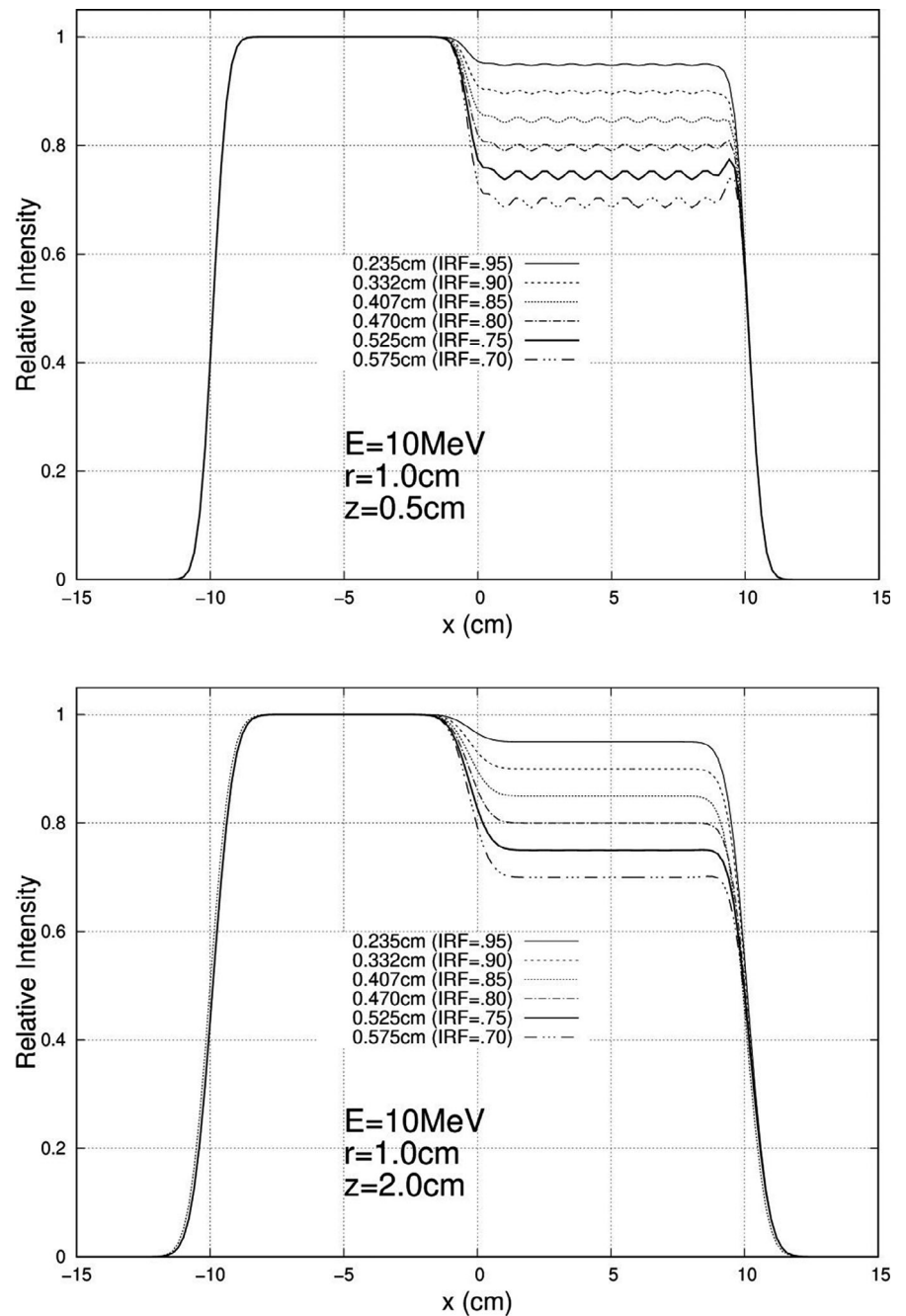


FIG. 6. Profiles at $y = 0$ cm for 10 MeV, 20×20 cm² half-modulated field ($r = 1.0$ cm), 103 cm source-to-surface distance (SSD): depth $z = 0.5$ cm (top) and $z = 2.0$ cm (bottom). The computed island block diameters (d) for 0.70, 0.75, 0.80, 0.85, 0.90, and 0.95 IRF values are listed in each plot's inserted key.

$$\text{IRF} = 1.0 - \frac{\pi}{2\sqrt{3}} \left(\frac{d}{r}\right)^2. \quad (1)$$

Hence, there are an infinite number of potential configurations for a single d/r ratio. Making d too small has the undesired effects of (1) requiring too many island blocks, likely increasing manufacturing costs, and (2) increasing the number of electrons scattering into and out of the blocks, which degrade the fluence distribution. Making d too large has the undesirable effect of not allowing sufficient electrons, via MCS, to fill in fluence behind the blocks, which causes hot and cold spots. Therefore, to achieve how best to deliver passive intensity modulation for IM-BECT, this study determined near-optimal values of island block separation (r) for patient-specific

conditions, that is, beam energy, source-to-surface distance (SSD), depth in water, and range of IRF values.

Using a pencil beam algorithm for electron fluence calculations and assuming perfect collimation (ie, ignoring MCS into and out of the island blocks and bremsstrahlung in the island blocks), we determined island block geometries (diameters and separations) for IRF values in the range of 70–95%, electron beams from 7 to 20 MeV ($R_{90} = 2.0, 2.5, 3.0, 3.5, 4.0, 5.0,$ and 6.0 cm), 100 and 103 cm SSD, and depths in water of 0.5 and 2.0 cm. Perfect collimation can be assumed because MCS into and from the island blocks and bremsstrahlung attenuation and production in the island blocks have only a small effect on the underlying dose distribution²³, which has

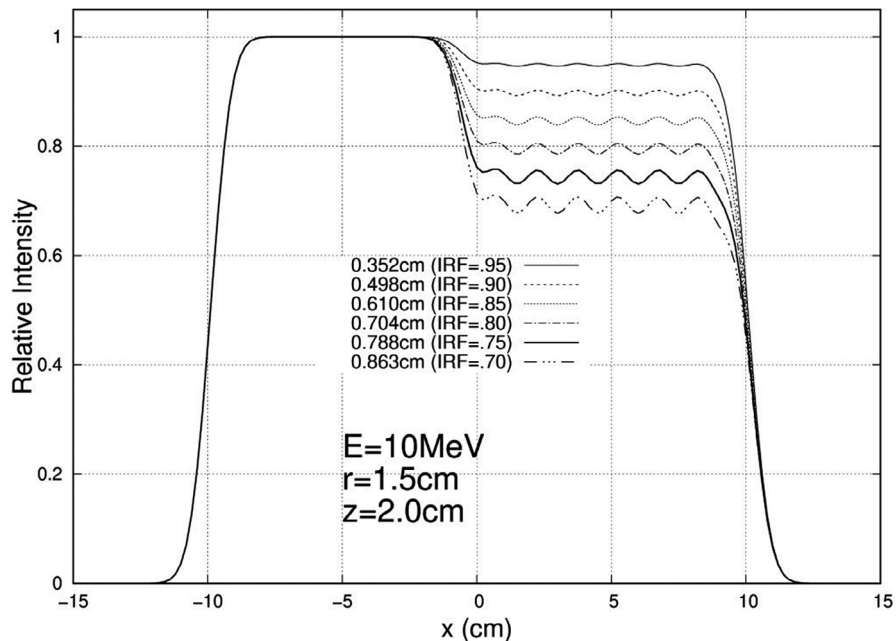
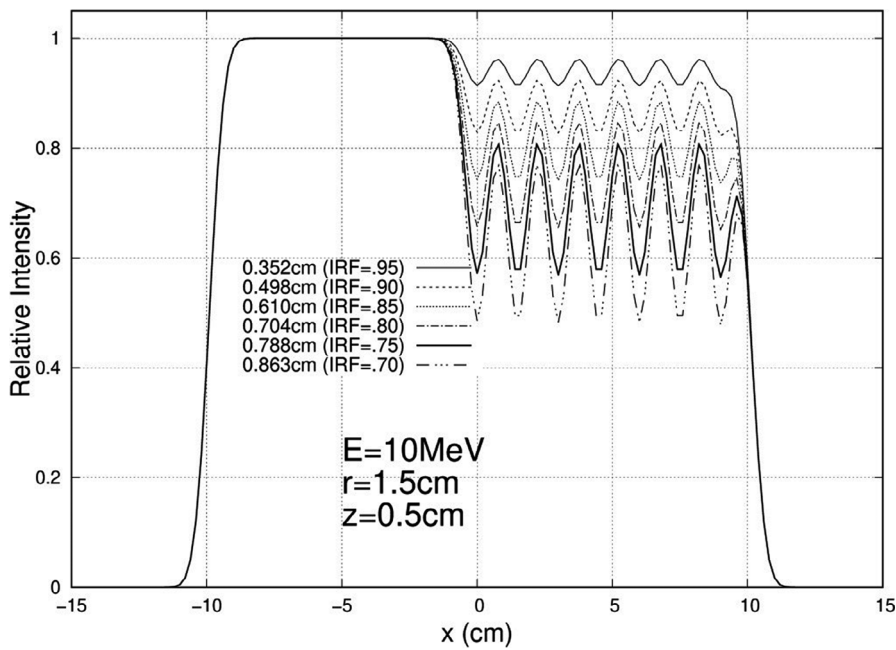


FIG. 7. Profiles at $y = 0$ cm for 10 MeV, 20×20 cm² half-modulated field ($r = 1.5$ cm), 103 cm source-to-surface distance (SSD): depth $z = 0.5$ cm (top) and $z = 2.0$ cm (bottom). The computed island block diameters (d) for 0.70, 0.75, 0.80, 0.85, 0.90, and 0.95 IRF values are listed in each plot's inserted key.

insignificant effect on selecting the near-optimal values of island block separation (r). Its impact on the underlying dose distribution, which can be a few percent²³, is otherwise important and will be reported in subsequent studies using Monte Carlo (MC) dose calculations to provide data for modifications to the PBRA, currently used for IM-BECT planning.

2 | METHODS

2.A | Conditions of study

Multiple island block geometries were studied for seven electron energies 7, 9, 10, 11, 13, 16, and 20 MeV. 100 cm and 103 cm SSD was

selected, as bolus ECT patients are typically treated at 105 cm source-to-skin surface distance (SSD_{skin}) to ensure the bolus does not collide with the applicator, which extends to 95 cm source-to-collimator distance (SCD). Bolus thickness typically averages approximately 2.0 cm, so that the SSD to the bolus surface is approximately 103 cm. The 100 cm SSD was selected as an upper limit where either the patient surface is closer to the source and/or a bolus thicker than 2.0 cm is required. Beam intensity modulation is intended to be reflected in the patient; therefore, we elected to study relative fluence (intensity) at depths of 0.5 cm and 2.0 cm in water. This resulted in 28 unique beam conditions studied (7 energies \times 2 SSDs \times 2 depths).

Based on Kudchadker et al.¹⁴ we studied IRF values of 0.70, 0.75, 0.80, 0.85, 0.90, and 0.95. We studied potentially practical

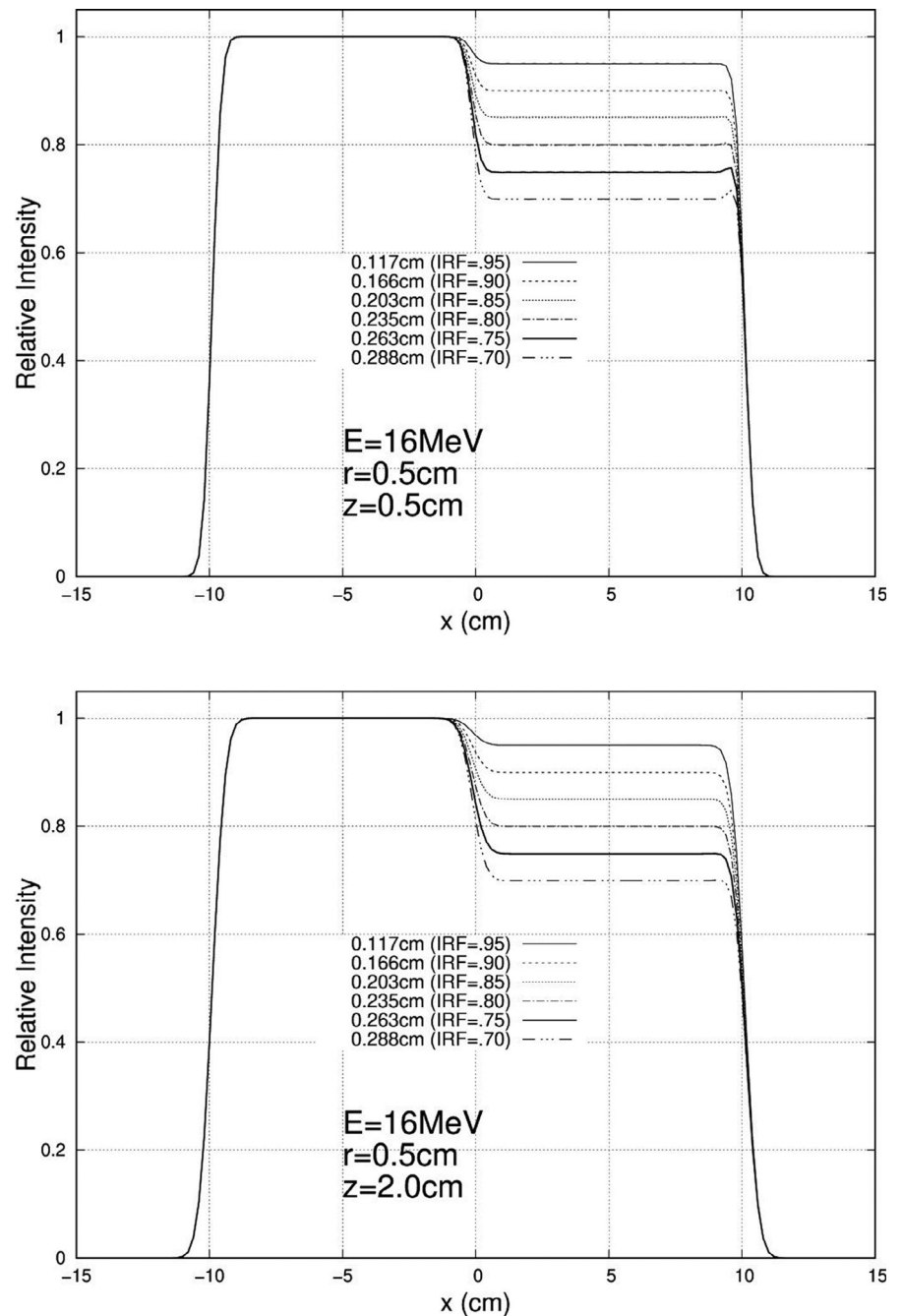


FIG. 8. Profiles at $y = 0$ cm for 16 MeV, 20×20 cm² half-modulated field ($r = 0.5$ cm), 103 cm source-to-surface distance (SSD): depth $z = 0.5$ cm (top) and $z = 2.0$ cm (bottom). The computed island block diameters (d) for 0.70, 0.75, 0.80, 0.85, 0.90, and 0.95 IRF values are listed in each plot's inserted key.

hexagonal separations for the island blocks of 0.50, 0.75, 1.00, 1.25, and 1.50 cm. Once a specific IRF and r are selected, d is determined using Eq. (1). These values, independent of beam conditions, are listed in Table 1 for 30 different IM configurations (6 IRF values \times 5 island block separations). Hence, relative fluence (intensity) distributions were calculated for 840 unique combinations (30 IM configurations \times 28 beam conditions).

2.B | Calculation of relative fluence distributions

Relative fluence was calculated in a plane perpendicular to central axis using the pencil beam algorithm (PBA) following the convention of Hogstrom et al,²⁴ assuming perfect collimation. The circular cross-

sections of the cylindrical island blocks were modeled as small square cross-sections of equal area. This calculation, detailed by Chambers,²⁵ was used to determine which block geometries (r and d) produce intensity distributions (70–95%) acceptable for clinical use. Calculations were performed for monoenergetic beams of energies 7, 9, 10, 11, 13, 16, and 20 MeV with σ_{θ_x} values of 0.069, 0.055, 0.050, 0.045, 0.040, 0.033, and 0.027 radians, respectively, using a 20×20 cm² field at depths of 0.5 cm and 2.0 cm. The collimating plane to water surface distances (air gaps) were taken to be 5 cm and 8 cm, corresponding to the 100 cm and 103 cm SSD, respectively, for a clinically divergent beam. Relative fluence profiles were calculated at the two depths in water for a 20×20 cm² field, which was half-covered by identical cylindrical island blocks placed

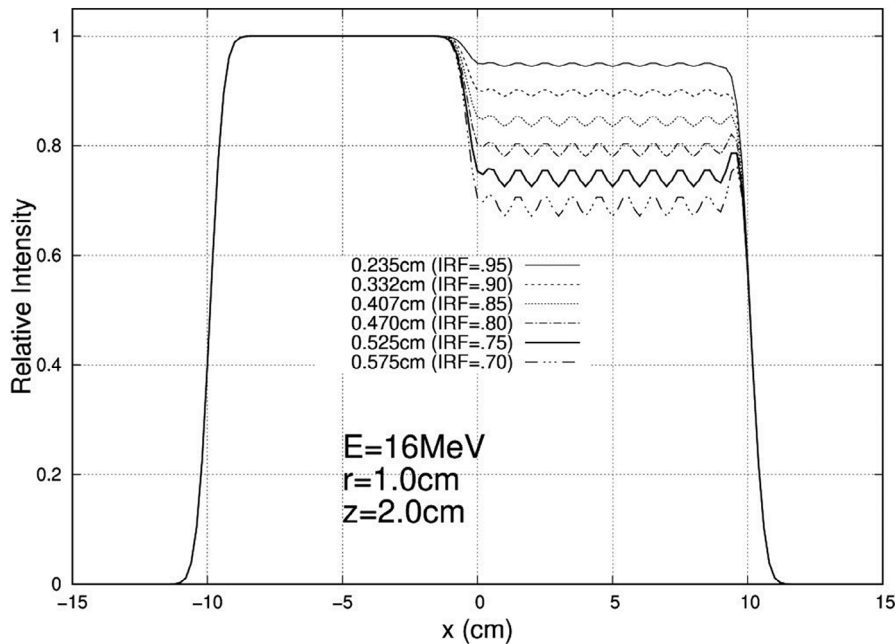
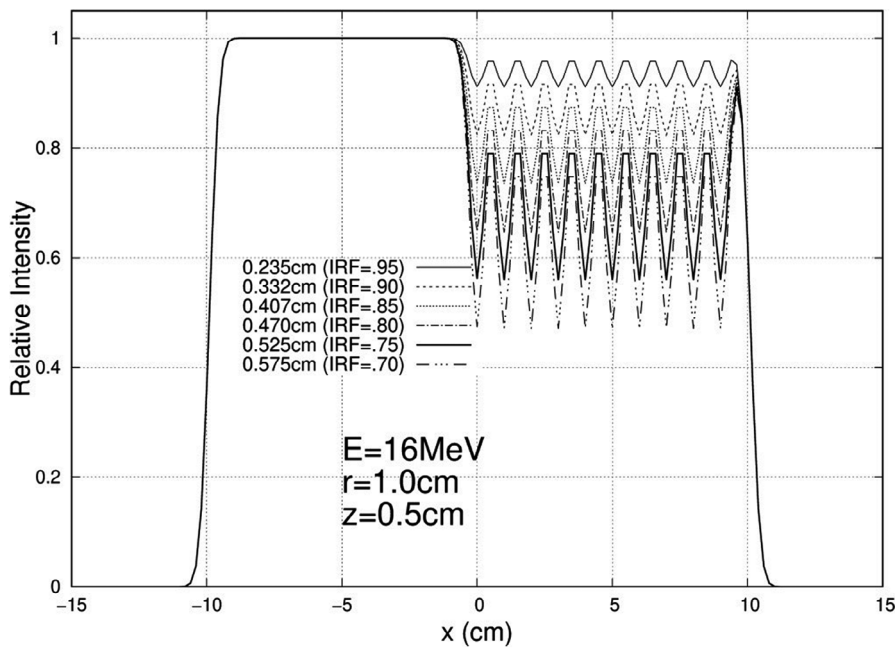


FIG. 9. Profiles at $y = 0$ cm for 16 MeV, 20×20 cm² half-modulated field ($r = 1.0$ cm), 103 cm source-to-surface distance (SSD): depth $z = 0.5$ cm (top) and $z = 2.0$ cm (bottom). The computed island block diameters (d) for 0.70, 0.75, 0.80, 0.85, 0.90, and 0.95 IRF values are listed in each plot's inserted key.

in a hexagonal array with separation r and block diameter d . A schematic of one such block matrix is shown in Fig. 3. Plots of relative fluence vs x position at $y = 0$ were generated. Each intensity modulator was assumed to be located in the 20×20 cm² block aperture, that is, 95 cm SSD.

2.C | Evaluation metrics

Calculated relative fluence (intensity) distributions downstream of the half-beam intensity modulators were evaluated using two metrics: average blocked intensity (I_{avg}) and ripple intensity (ΔI_R). I_{avg} was the average intensity for $|y| < 7.5$ cm and $2.5 \leq x \leq 7.5$ cm. ΔI_R was defined as the difference between the maximum and minimum

intensities within the blocked region, defined by $|y| < 7.5$ cm and $2.5 \leq x \leq 7.5$ cm. A block configuration (r, d) for each energy, was considered unacceptable if I_{avg} differed from the intended IRF by more than 2% or if ΔI_R was greater than 4%, which was always symmetric ($\pm 2\%$) about I_{avg} . Criteria for these first two metrics require all intensities to be within 4% of the intended intensity; however, as results will show, I_{avg} was always within 0.1%, so that all intensities would be within $\pm 2\%$ of the intended intensity. Also, a third metric called distance of transition (d_T) was calculated for all combinations. d_T was defined as the average straight-line distance along the x -axis from relative intensities 0.99 to IRF + 0.01 for each x profile (every 0.2 cm in y) such that $|y| < 7.5$ cm. This distance is a measure of the spatial resolution of the specific IRF, that

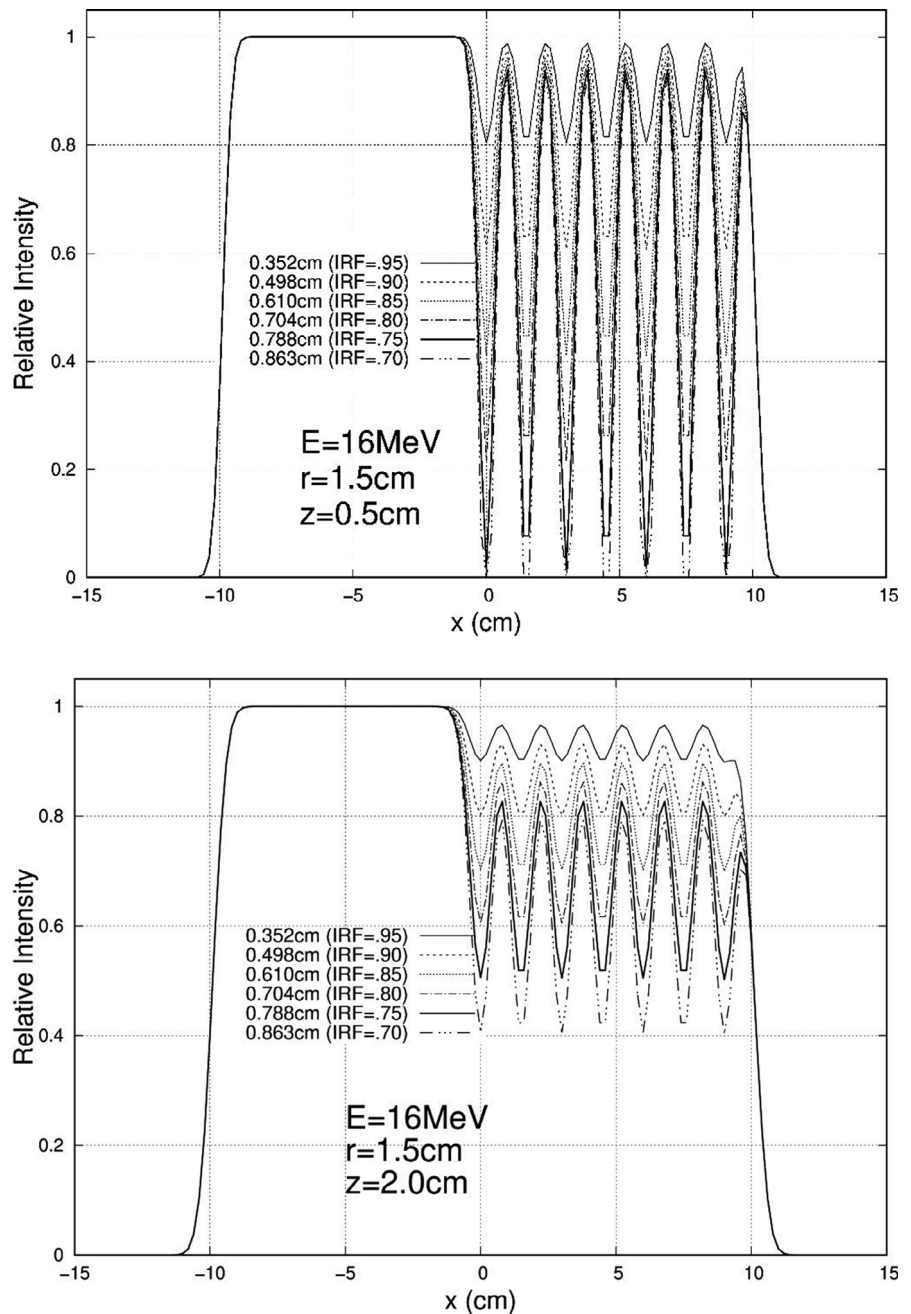


FIG. 10. Profiles at $y = 0$ cm for 16 MeV, 20×20 cm² half-modulated field ($r = 1.5$ cm), 103 cm source-to-surface distance (SSD): depth $z = 0.5$ cm (top) and $z = 2.0$ cm (bottom). The computed island block diameters (d) for 0.70, 0.75, 0.80, 0.85, 0.90, and 0.95 IRF values are listed in each plot's inserted key.

is, the distance required to modify the intensity. Fig. 4 illustrates these three metrics.

3 | RESULTS AND DISCUSSION

3.A | Intensity profiles and metrics

Calculations were performed and plotted for each of the 840 unique combinations specified above, and exemplary results are plotted here. For 10 MeV, Figs. 5, 6, and 7 show relative intensity vs x profiles at $y = 0$ for hexagonal separations $r = 0.5$, 1.0, and 1.5 cm respectively for each IRF (0.70, 0.75, 0.80, 0.85, 0.90, and 0.95) at calculation depths (z) of 0.5 cm and 2.0 cm for

103 cm SSD. Similar results at 16 MeV are shown in Figs. 8, 9, and 10, respectively. The complete set of $y = 0$ profiles for all r (0.5, 0.75, 1.0, 1.25, and 1.5 cm) and IRF (0.70, 0.75, 0.80, 0.85, 0.90, and 0.95) combinations at all energies (7, 9, 10, 11, 13, 16, and 20 MeV), both SSDs (100 and 103 cm), and both depths (0.5 and 2.0 cm) is documented in Appendix B of Chamber's thesis.²⁵

These relative electron intensity x -profiles were scored and evaluated using the three metrics I_{avg} , ΔI_R , and d_T , as previously defined in Section 2.C. Tables 2 and 3 show the scoring values for the 10 MeV and 16 MeV distributions, respectively, at 103 cm SSD. Tables for all seven energies and two SSDs are documented in Appendix C of Chambers' thesis.²⁵

TABLE 2 Metrics summary for 10 MeV at 103 cm source-to-surface distance (SSD) at $y = 0$ cm 20×20 cm² half-modulated field for $z = 0.5$ cm (middle columns) and $z = 2.0$ cm (right columns).

r (cm)	IRF	d (cm)	z = 0.5 cm			z = 2.0 cm		
			d _T	I _{avg}	ΔI _R	d _T	I _{avg}	ΔI _R
0.5	0.95	0.117	0.63	0.950	0.000	1.05	0.950	0.000
	0.90	0.166	1.03	0.900	0.000	1.66	0.900	0.000
	0.85	0.203	1.42	0.851	0.000	1.87	0.851	0.000
	0.80	0.235	1.42	0.800	0.000	2.07	0.800	0.000
	0.75	0.263	1.43	0.749	0.000	2.26	0.749	0.000
	0.70	0.288	1.62	0.699	0.000	2.27	0.699	0.000
0.75	0.95	0.176	0.79	0.950	0.000	1.15	0.950	0.000
	0.90	0.249	1.16	0.900	0.000	1.67	0.900	0.000
	0.85	0.305	1.22	0.850	0.000	2.02	0.850	0.000
	0.80	0.352	1.42	0.800	0.000	2.07	0.800	0.000
	0.75	0.394	1.58	0.750	0.000	2.81	0.750	0.000
	0.70	0.431	1.62	0.701	0.001	2.44	0.701	0.000
1	0.95	0.235	0.67	0.950	0.004	1.04	0.950	0.000
	0.90	0.332	1.03	0.900	0.007	1.61	0.900	0.000
	0.85	0.407	1.24	0.850	0.011	1.53	0.850	0.000
	0.80	0.470	1.30	0.800	0.015	2.03	0.800	0.000
	0.75	0.525	1.47	0.750	0.019	2.17	0.750	0.000
	0.70	0.575	1.64	0.700	0.022	2.26	0.700	0.000
1.25	0.95	0.294	0.69	0.950	0.021	0.98	0.950	0.001
	0.90	0.415	1.98	0.900	0.042	1.59	0.900	0.002
	0.85	0.508	2.27	0.850	0.063	1.78	0.850	0.002
	0.80	0.587	2.20	0.800	0.084	2.02	0.800	0.003
	0.75	0.656	2.24	0.750	0.104	2.12	0.750	0.004
	0.70	0.719	2.26	0.700	0.125	2.19	0.700	0.005
1.5	0.95	0.352	2.50	0.950	0.053	0.95	0.950	0.006
	0.90	0.498	2.51	0.901	0.106	1.43	0.900	0.011
	0.85	0.610	2.65	0.851	0.159	1.94	0.850	0.017
	0.80	0.704	2.50	0.802	0.212	2.18	0.800	0.022
	0.75	0.788	2.42	0.752	0.266	2.61	0.750	0.028
	0.70	0.863	2.45	0.702	0.319	2.74	0.700	0.034

3.B | Evaluation of I_{avg}

I_{avg} agrees within 0.001 of the intended values (0.70, 0.75, 0.80, 0.85, 0.90, and 0.95) for all combinations of beam energy, SSD, z, r, and IRF values, providing ΔI_R values are less than 0.10, which is well outside our acceptable criteria of 0.04. Hence, the I_{avg} acceptance criterion is redundant and unnecessary, as expected, as I_{avg} should equal the fraction of the beam unblocked by the island blocks. Furthermore, this reinforces the utility of passive intensity modulation using island blocks for IM-BECT.

3.C | Evaluation of ΔI_R

Ripple intensity trends smaller for lower energy, smaller block separation, and larger IRFs (nearer 1.0). A practical utilization of these

data was to determine what are acceptable r values, that is, maximum block separation (r_{max}), for a specific set of conditions, namely energy, SSD, and IRF_{min}, the latter being the minimum value for a specific patient's planned intensity distribution. As previously discussed, larger acceptable r values are more advantageous. Therefore, one preferred criterion might be to select the largest r value that keeps ΔI_R ≤ 4% at z = 2.0 cm. Data for z = 0.5 cm produce substantially greater ΔI_R values, which require progressively smaller r values if the shallow depth oscillations are in the patient, as opposed to being in the bolus. Further analysis of results is restricted to 103 cm SSD, since this is more typical of the clinic.

These data are also useful for estimating the maximum island block separation for a given patient IM-BECT geometry, which allows the fewest number of island blocks and the largest island block diameters, minimizing cost and effect of electron scatter into

TABLE 3 Metrics summary for 16 MeV at 103 cm source-to-surface distance (SSD) at $y = 0$ cm 20×20 cm² half-modulated field for $z = 0.5$ cm (middle columns) and $z = 2.0$ cm (right columns).

r (cm)	IRF	d (cm)	z = 0.5 cm			z = 2.0 cm		
			d_T	I_{avg}	ΔI_R	d_T	I_{avg}	ΔI_R
0.5	0.95	0.117	0.56	0.950	0.042	0.63	0.950	0.000
	0.90	0.166	0.61	0.900	0.007	1.03	0.900	0.000
	0.85	0.203	0.94	0.854	0.001	1.22	0.851	0.000
	0.80	0.235	1.00	0.800	0.000	1.42	0.800	0.000
	0.75	0.263	1.00	0.749	0.001	1.42	0.749	0.000
	0.70	0.288	1.00	0.699	0.001	1.42	0.699	0.000
0.75	0.95	0.176	0.44	0.950	0.024	0.68	0.950	0.000
	0.90	0.249	0.73	0.900	0.031	1.03	0.900	0.001
	0.85	0.305	1.38	0.850	0.033	1.22	0.850	0.001
	0.80	0.352	1.55	0.800	0.044	1.25	0.800	0.001
	0.75	0.394	2.35	0.750	0.056	1.39	0.750	0.001
	0.70	0.431	1.90	0.700	0.067	1.48	0.701	0.002
1	0.95	0.235	1.17	0.950	0.056	0.59	0.950	0.007
	0.90	0.332	0.86	0.900	0.113	1.23	0.900	0.014
	0.85	0.407	1.54	0.850	0.169	1.37	0.850	0.021
	0.80	0.470	1.68	0.800	0.226	1.55	0.800	0.029
	0.75	0.525	1.50	0.751	0.282	1.90	0.750	0.036
	0.70	0.575	1.50	0.701	0.338	2.21	0.700	0.043
1.25	0.95	0.294	1.19	0.950	0.112	1.07	0.950	0.032
	0.90	0.415	1.29	0.901	0.243	2.09	0.900	0.064
	0.85	0.508	1.43	0.851	0.363	1.98	0.850	0.095
	0.80	0.587	1.50	0.801	0.485	2.10	0.800	0.127
	0.75	0.656	1.55	0.752	0.606	2.17	0.751	0.159
	0.70	0.719	1.56	0.702	0.728	2.17	0.700	0.191
1.5	0.95	0.352	0.67	0.951	0.191	2.20	0.951	0.071
	0.90	0.498	0.69	0.903	0.382	2.48	0.901	0.143
	0.85	0.610	0.97	0.854	0.573	2.40	0.852	0.214
	0.80	0.704	0.97	0.806	0.763	2.60	0.802	0.285
	0.75	0.788	0.99	0.757	0.955	2.54	0.752	0.357
	0.70	0.863	0.98	0.712	0.967	2.41	0.703	0.428

and from the island blocks. First, plots of ΔI_R vs r (cm) for multiple combinations of energies (11, 13, 16, and 20 MeV) and IRF values (0.70, 0.80, and 0.90) can be made for each of the four possible SSD and depths combinations. From these plots, the maximum island block separation (r_{max}) can be extracted and plotted vs the IRF. Resulting plots are exemplified in Fig. 11 for the highest three energies (13, 16, and 20 MeV). Using these plots, based on beam energy and IRF_{min} , a maximum island block separation value (r_{max}) can be selected for use with a specific patient. For example, for the 16 MeV beam, 103 cm SSD, and 2.0 cm depth, an IRF_{min} of 0.85 has an r_{max} of 1.09 cm. It should be understood that the island block separation (r) can be decreased from r_{max} as needed for desired uniformity in individual patient plans.

3.D | Evaluation of d_T

Though d_T had no formal pass/fail limit, for clinical use, the smallest d_T is preferred because it is a measure of how rapidly intensity could be modulated. Table 4 summarizes d_T values for a representative subset of all studied geometries at 103 cm SSD. From these results, it can be concluded that d_T trends smaller for higher energy, smaller SSD, shallower depth, just as penumbra widths at beam edges trend. Also, d_T trends smaller for IRF values closer to 1.0, simply a result of a gradient changing less over a shorter distance.

Distance of transition monotonically decreased with energy, following an approximately $1/E$ dependence, similar to that of σ_{0x} . This is illustrated by Fig. 12, which plots results at $z = 0.5$ and 2.0 cm for

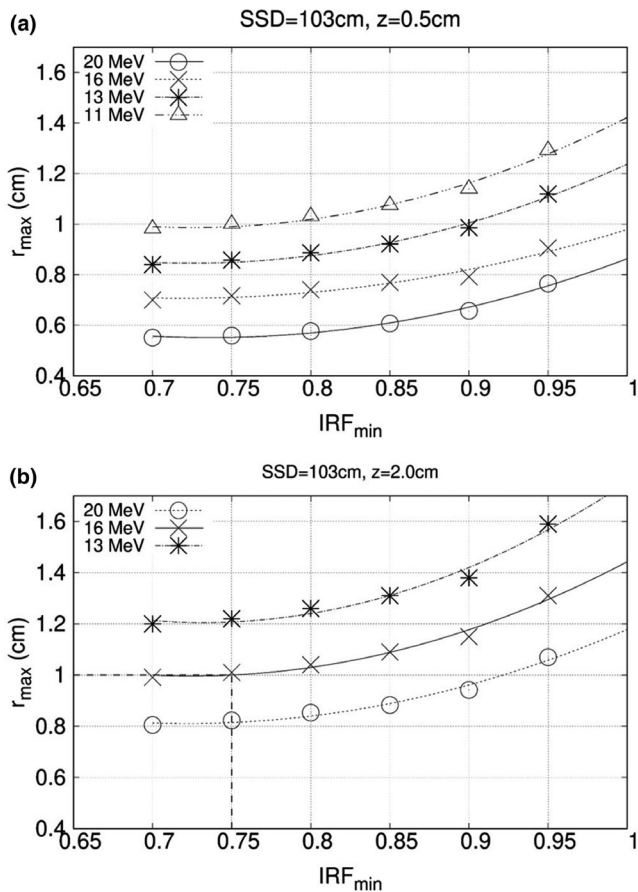


FIG. 11. Maximum island block separation (r_{\max}) vs minimum IRF value in intensity-modulated field (IRF_{\min}) for which I_R is the maximum acceptable value, 4%. Plots are at specified beam energies (see inserted key) for 103 cm source-to-surface distance (SSD) and (a) depth $z = 0.5$ cm and (b) depth $z = 2.0$ cm, the latter corresponding to an average bolus thickness of 2 cm. For example, for conditions in (b) at 16 MeV and IRF_{\min} value of 0.75 requires an island block separation less than 1.0 cm (as indicated by the dashed line). Curves are quadratic fits to data points.

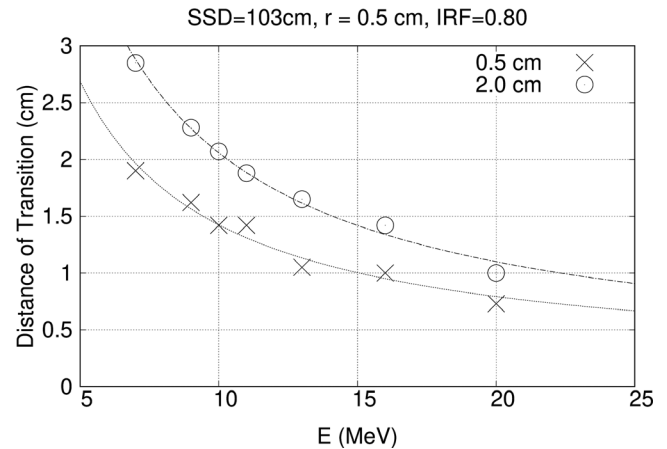


FIG. 12. Distance of transition (d_T) vs beam energy (E) and depth for 103 cm source-to-surface distance (SSD), $r = 0.5$ cm, and $IRF = 0.80$. Data at depth 0.5 cm (Xs); data at depth 2.0 cm (circles). For a given IRF and at both depths, d_T monotonically decreased with increased energy. Curves have been fit with a $1/E$ dependence.

$r = 0.5$ cm and $IRF = 0.80$. The values at $z = 0.5$ cm are about 70% of those of $z = 2.0$ cm.

Not surprisingly, d_T was approximately constant with variation in r (0.5–1.5 cm), so long as ΔI_R (variation in IRF) was less than 2%. For

TABLE 4 Distance of Transition (d_T) in cm for half-beam intensity modulators (cf Fig. 3) in water at 103 cm source-to-surface distance (SSD) and depths of 0.5 cm (left) and 2.0 cm (right).

SSD = 103 cm Depth = 0.5 cm				SSD = 103 cm Depth = 2.0 cm			
7 MeV				7 MeV			
IRF	$r = 0.5$ cm	$r = 1.0$ cm	$r = 1.5$ cm	IRF	$r = 0.5$ cm	$r = 1.0$ cm	$r = 1.5$ cm
0.90	1.49	1.56	1.33	0.90	2.19	2.18	2.12
0.80	1.90	1.95	2.61	0.80	2.85	2.84	2.77
0.70	2.26	2.18	2.98	0.70	3.24	3.22	3.11
13 MeV				13 MeV			
IRF	$r = 0.5$ cm	$r = 1.0$ cm	$r = 1.5$ cm	IRF	$r = 0.5$ cm	$r = 1.0$ cm	$r = 1.5$ cm
0.90	1.00	1.68	2.00	0.90	1.26	1.24	2.50
0.80	1.05	1.82	1.86	0.80	1.65	1.58	2.70
0.70	1.26	1.85	1.82	0.70	1.83	1.75	2.70
20 MeV				20 MeV			
IRF	$r = 0.5$ cm	$r = 1.0$ cm	$r = 1.5$ cm	IRF	$r = 0.5$ cm	$r = 1.0$ cm	$r = 1.5$ cm
0.90	0.64	0.92	0.88	0.90	0.89	1.27	1.79
0.80	0.73	1.06	1.13	0.80	1.00	1.54	1.75
0.70	0.89	1.21	0.74	0.70	1.20	1.61	1.66

Tables show data at beam energies of 7 MeV (top), 13 MeV (middle), and 20 MeV (bottom). d_T is shown for combinations of three IRF values (0.70, 0.80, and 0.90) and three hexagonal island block separations (0.5, 1.0, and 1.5 cm). d_T values have an estimated error of 0.05 cm. Clinically viable combinations ($\Delta I_R \leq 4\%$) (cf Tables 5, 6) are bolded for clarity.

TABLE 5 Range of intensity reduction factors (IRF ≥ 0.70) of half-beam intensity modulators (cf Fig. 3) that meet acceptability criteria ($\Delta I_R \leq 4\%$) at 100 cm source-to-surface distance (SSD) and depths in water of $z = 0.5$ cm (top) and $z = 2.0$ cm (bottom).

SSD = 100 cm Depth = 0.5 cm					
E (MeV)	r = 0.5 cm	r = 0.75 cm	r = 1.0 cm	r = 1.25 cm	r = 1.5 cm
7	✓	✓	0.80	0.95	N/A
9	✓	✓	0.95	N/A	N/A
10	✓	0.85	N/A	N/A	N/A
11	✓	0.95	N/A	N/A	N/A
13	✓	N/A	N/A	N/A	N/A
16	0.85	N/A	N/A	N/A	N/A
20	N/A	N/A	N/A	N/A	N/A
SSD = 100 cm Depth = 2.0 cm					
E (MeV)	r = 0.5 cm	r = 0.75 cm	r = 1.0 cm	r = 1.25 cm	r = 1.5 cm
7	✓	✓	✓	✓	✓
9	✓	✓	✓	✓	0.85
10	✓	✓	✓	0.75	0.95
11	✓	✓	✓	0.90	N/A
13	✓	✓	0.80	0.95	N/A
16	✓	✓	0.95	0.95	N/A
20	✓	0.90	N/A	N/A	N/A

Beam energies (E).

Hexagonal separation (r).

Check marks demarcate acceptability of all island blocks for IRF ≥ 0.70 .

Fractional numbers indicate the smallest IRF studied that meets acceptability criteria.

N/A indicated no IRF ≥ 0.70 met acceptability criteria.

TABLE 6 Range of intensity reduction factors (IRF ≥ 0.70) of half-beam intensity modulators (cf Fig. 3) that meet acceptability criteria ($\Delta I_R \leq 4\%$) at 103 cm source-to-surface distance (SSD) and depths in water of $z = 0.5$ cm (top) and $z = 2.0$ cm (bottom).

SSD = 103 cm Depth = 0.5 cm					
E (MeV)	r = 0.5 cm	r = 0.75 cm	r = 1.0 cm	r = 1.25 cm	r = 1.5 cm
7	✓	✓	✓	✓	0.80
9	✓	✓	✓	0.85	0.95
10	✓	✓	✓	0.95	N/A
11	✓	✓	✓	0.95	N/A
13	✓	✓	0.95	N/A	N/A
16	✓	0.85	N/A	N/A	N/A
20	✓	0.95	N/A	N/A	N/A
SSD = 103 cm Depth = 2.0 cm					
E (MeV)	r = 0.5 cm	r = 0.75 cm	r = 1.0 cm	r = 1.25 cm	r = 1.5 cm
7	✓	✓	✓	✓	✓
9	✓	✓	✓	✓	✓
10	✓	✓	✓	✓	✓
11	✓	✓	✓	✓	0.85
13	✓	✓	✓	0.80	0.95
16	✓	✓	0.75	0.95	N/A
20	✓	✓	0.95	N/A	N/A

Beam energies (E).

Hexagonal separation (r).

Check marks demarcate acceptability of all island blocks for IRF ≥ 0.70 .

Fractional numbers indicate the smallest IRF studied that meets acceptability criteria.

N/A indicated no IRF ≥ 0.70 met acceptability criteria.

example, for an IRF of 0.80 at 11 MeV and for $z = 0.5$ cm and $z = 2.0$ cm, d_T remained within 0.1 cm of an average of 1.32 and 1.89 cm, respectively.

3.E | Combinations (r,d) suitable for clinical use

Table 5 summarizes the scoring results at 100 cm SSD for all combinations (E, r) at depths $z = 0.5$ cm and $z = 2.0$ cm for all IRF values (0.70-0.95). Combinations with a check denote those passing both I_{avg} and I_R criteria for all IRF (>0.70), which are acceptable for intensity modulator design. For partial passes, the minimum permissible IRF is given, and where no modulation (IRF ≥ 0.70) is possible, the combination is marked "not acceptable" (N/A).

At shallow depths ($z = 0.5$ cm), the results show that beam energies above 13 MeV do not exhibit sufficient scatter to produce clinically acceptable intensity distributions for the entire range of IRFs under consideration. In particular, 20 MeV beams may not be used under any conditions, and 16 MeV is limited to a minimum IRF of 0.85. For a deeper matching depth ($z = 2.0$ cm), beam energies up to and including 20 MeV can be used.

Table 6 summarizes the scoring results at 103 cm SSD for all combinations (E, r) at depths $z = 0.5$ cm and $z = 2.0$ cm for all IRF (0.70-0.95), respectively. At this more clinical SSD, beam energies from 7 to 20 MeV have acceptable geometries for all IRF. In general, the 103 cm SSD allows larger block diameters, which as previously mentioned, have advantages.

4 | SUMMARY AND CONCLUSION

The objective of this study was to determine combinations of block diameter and hexagonal grid separation, which could be used to produce clinically acceptable intensity distributions for IM-BECT, while minimizing ΔI_R and d_T . A pencil beam algorithm was used to calculate the relative fluence (intensity) distribution beneath a half-modulated 20×20 cm² field (island blocks on positive x-axis) for a range of hexagonal separations (0.5–1.5 cm) and IRFs (0.70–0.95), having island block diameters ($d = 0.117$ – 0.863 cm) at depths of $z = 0.5$ cm and $z = 2.0$ cm. This was done both at 100 cm SSD (air gap = 5.0 cm) and at an extended 103 cm SSD (air gap = 8.0 cm) for beam energies of 7–20 MeV.

Results showed that (1) the average intensity agreed with the intended intensity within 0.001 as long as ΔI_R was within a clinically acceptable range (≤ 0.04) and (2) ΔI_R was clinically acceptable in limited regions of E, SSD, r, IRF, and z space. For example, the use of 20 MeV beams was precluded at 100 cm SSD and shallow depth ($z = 0.5$ cm), and the 16 MeV beam was limited to cases with IRF ≥ 0.85 . However, using a more clinical 103 cm SSD, ΔI_R was acceptable for all energies (7–20 MeV) and depths ($z = 0.5$ and 2.0 cm). Also, the data provided plots for specific conditions from which the maximum island block separation (r_{max}) could be extracted.

Although selecting solutions with the largest block separation (r) and thus the largest diameter blocks may have some fabrication and

block scatter advantages, this comes with the disadvantage of slightly increased distance of transition (d_T), which could limit the gradient of sharply varying intensity-modulating patterns. If necessary, these competing effects can be properly balanced in the planning process, which will depend on the wide range of data computed for this study.

We conclude that these data are useful in determining island block hexagonal separation and hence island block diameters required to produce electron beam intensity modulators for individual patients receiving IM-BECT.

REFERENCES

- Hogstrom KR, Almond PR. Review of electron beam therapy physics. *Phys Med Biol*. 2006;51(13):R455-R489.
- Haas LL, Harvey RA, Laughlin JS, Beattie JW, Henderson WJ. Medical aspects of high energy electron beams. *Am J Roentgenol Radium Ther Nucl Med*. 1954;72:250-259.
- Tapley ND. *Clinical Application of the Electron Beam*. New York, NY: Wiley Biomedical; 1976.
- Vaeth JM, Meyer JL. *The Role of High Energy Electrons in the Treatment of Cancer: Frontiers of Radiation Therapy and Oncology*, vol. 25. San Francisco, CA: Karger; 1991.
- Gerbi BJ, Antolak JA, Deibel FC et al Recommendations for clinical electron beam dosimetry: supplement to the recommendations of Task Group 25. *Med Phys*. 2009;36(7):3239-3279.
- Hogstrom KR, Antolak JA, Kudchadker RJ, Ma CMC, Leavitt DD. Modulated electron therapy. In: Palta J, Mackie R, eds. *Intensity Modulated Radiation Therapy, The State of the Art: Proceedings of the 2003 AAPM Summer School*. Madison, WI: Medical Physics Publishing; 2003:749-786.
- Low DA, Starkschall G, Bujnowski SW, Wang L, Hogstrom KR. Electron bolus design for radiotherapy treatment planning: bolus design algorithms. *Med Phys*. 1992;19:115-124.
- Su S, Moran K, Robar JL. Design and production of 3D printed bolus for electron radiation therapy. *J Appl Clin Med Phys*. 2014;15:194-211.
- Shiu AS, Hogstrom KR. Pencil-beam redefinition algorithm for electron dose distributions. *Med Phys*. 1991;18:7-18.
- Boyd RA, Hogstrom KR, Rosen I. Effect of using an initial polyenergetic spectrum with the pencil-beam redefinition algorithm for electron-dose calculations in water. *Med Phys*. 1998;25:2176-2185.
- Boyd RA, Hogstrom KR, Starkschall G. Electron pencil-beam redefinition algorithm dose calculations in the presence of heterogeneities. *Med Phys*. 2001;28:2096-2104.
- Carver RL, Hogstrom KR, Chu C, Fields RS, Sprunger CP. Accuracy of pencil-beam redefinition algorithm dose calculations in patient-like cylindrical phantoms for bolus electron conformal therapy. *Med Phys*. 2013;40:071720.
- Low DA, Starkschall G, Sherman NE, Bujnowski SW, Ewton JR, Hogstrom KR. Computer-aided design and fabrication of an electron bolus for treatment of the paraspinal muscles. *Int J Radiat Oncol Biol Phys*. 1995;33:1127-1138.
- Kudchadker RJ, Hogstrom KR, Garden AS, McNeese MD, Boyd RA, Antolak JA. Electron conformal radiotherapy with bolus and intensity modulation. *Int J Radiation Oncology Biol Phys*. 2002;53:1023-1037.
- Perkins GH, McNeese MD, Antolak JA, Buchholz TA, Strom EA, Hogstrom KR. A custom three-dimensional electron bolus technique for optimization of postmastectomy irradiation. *Int J Radiat Oncol Biol Phys*. 2001;51:1142-1151.

16. Kim MM, Kudchadker RJ, Kanke JE, Zhang S, Perkins GH. Bolus electron conformal therapy for the treatment of recurrent inflammatory breast cancer: a case report. *Med Dosim*. 2012;37:208-213.
17. Opp D, Forster K, Li W, Zhang G, Harris EE. Evaluation of bolus electron conformal therapy compared with conventional techniques for the treatment of left chest wall postmastectomy in patients with breast cancer. *Med Dosim*. 2013;38:448-453.
18. Kudchadker RJ, Antolak JA, Morrison WH, Wong PF, Hogstrom KR. Utilization of custom electron bolus in head and neck radiotherapy. *J Appl Clin Med Phys*. 2003;4:321-333.
19. Zeidan OA, Chauhan BD, Estabrook WW, Willoughby TR, Manon RR, Meeks SL. Image-guided bolus electron conformal therapy- a case study. *J Appl Clin Med Phys*. 2001;12(1):68-75.
20. Hogstrom KR, Boyd RA, Antolak JA, Svatos MM, Faddegon BA, Rosenman JG. Dosimetry of a prototype retractable eMLC for fixed-beam electron therapy. *Med Phys*. 2004;31:443-462.
21. Gauer T, Albers D, Cremers F, Harmansa R, Pelligrini R, Schmidt R. Design of a computer controlled multileaf collimator for advanced electron radiotherapy. *Phys Med Biol*. 2006;51:5987-6003.
22. Hogstrom KR, Carver RL, Chambers EL, Erhart K. Introduction to passive electron intensity modulation. *J Appl Clin Med Phys*. 2018;18(6):10-19.
23. Hilliard EN. *Verification and evaluation of a passive intensity modulation device for bolus electron conformal therapy*. Masters Thesis. Baton Rouge, LA: Louisiana State University; 2018.
24. Hogstrom KR, Mills MD, Almond PR. Electron beam dose calculations. *Phys Med Biol*. 1981;26(3):445-459.
25. Chambers EL. *Design of a passive intensity modulation device for bolus electron conformal therapy*. Masters Thesis. Baton Rouge, LA: Louisiana State University; 2016.